Weimin Chen[1]
Key Laboratory of Mechanics in Fluid Solid Coupling System,
Institute of Mechanics,
Chinese Academy of Sciences,
Beijing 100190, China
e-mail: wmchen@imech.ac.cn

Min Li
School of Aeronautics Sciences and Engineering,
Beijing University of Aeronautics and Astronautics,
Beijing 100191, China
e-mail: limin@buaa.edu.cn

Liwu Zhang
Key Laboratory of Mechanics in Fluid Solid Coupling System,
Institute of Mechanics,
Chinese Academy of Sciences,
Beijing 100190, China

Tiancai Tan
School of Aeronautics Sciences and Engineering,
Beijing University of Aeronautics and Astronautics,
Beijing 100191, China

Study on Multimode Vortex-Induced Vibration of Deepwater Riser in Different Flow Fields by Finite Element Simulations

Multimode vortex-induced vibration (VIV) of slender risers, respectively, in stepped and shear flows is explored by finite element simulations. Taking account of the interaction-between fluid and structure, a hydrodynamic model is proposed and embedded into the finite element simulation so as to carry out dynamic response of multimode VIV in time-domain. Multimode VIV in both stepped and shear flow fields is examined. In the case of stepped flow, a semi-empirical formula of modal weight is given. In the case of shear flow, modal excitation region can be determined based on modal energy, and partic-ipating modes approximately distribute in scattering groups. [DOI: 10.1115/1.4031729]

1 Introduction

With the development of oil and gas exploration toward to deeper sea, more deepwater platforms, such as spar, tension leg, and semisubmersible platforms, have been put into services. The marine riser of these platforms is used to transport gas and oil or optical and electrical information. The wake fluid field, body motion, and interaction between fluid and solid body of these slender risers experiencing nonuniform ocean flow become more complicated as water depth increases. For example, the shedding mode or frequency of wake vortex will vary along the riser length, rather than keeping constant. Additionally, the dynamic characteristics of slender riser usually present low-frequency and high-density natural modes due to large structural flexibility. Therefore, the VIV of a slender riser experiencing nonuniform flow often presents new phenomena [1–6], such as multimode, traveling wave, and wide-band random vibrations. These phenomena have presented new challenges to practical engineers and researchers.

In recent years, large numbers of large-scale field experiments and computational fluid dynamics simulations of slender riser VIV were implemented [7–13]. And, mechanism studies and empirical formula based on these large-scale experiments have been prosperously developed. Among these researches, the multimode vibration and drag coefficient in Ref. [6], high-mode lock-in in Ref. [12], and modal weight in Refs. [7] and [13] provided fruitful bases for the understanding and prediction of multimode VIV.

As we know, in the case of single-mode VIV, the modal excitation location can be simply determined as long as the modal reduced velocity $V_{rn}(z,n) = V(z)/Df_n$ at location z along the riser length falls into the range of lock-in velocity, i.e., $4 \le V_{rn}(z) \le 12$. However, in the case of multimode vibration, at length location z, there may exist multiple participating modes of which the modal reduced velocities satisfy $4 \le V_{rn}(z) \le 12$. In other words, overlap between adjacent excitation regions may appear if several modes simultaneously participate in the vibration. To eliminate the overlap, two methods are currently used. One method (referred as the high-mode priority [4,14] in the later part of this paper) assumes that the region of lower mode be covered by the region of higher mode. According to this method, if a riser undergoes uniform flow field, only the highest mode can participate in the vibration because other lower modes are covered by the highest mode. Or, the vibration will be single-mode response. But, some experiments [15,16] indicate that multimode VIV can occur even though the flow velocity along the riser is uniform.

Another method [12] (referred to as the equally shrinking later) assumes that the excitation region length of each mode involved in the overlap shrinks equally until the overlap is eliminated. Through the modal analysis based on the data of large-scale VIV tests, we found that there exist competitions between potential exciting modes. For example, VIV experiments [17] imply that the participating modes may vary with the variation of reduced velocity, moreover, appearance of new excitation mode is usually accompanied with disappearance of existing vibrating modes. Or, the new excitation mode with increasingly larger power of competition may overcome the previous one with decreasing power until it disappears in dynamic response. Additionally, observing large-scale tests in shear flow [13], we found that the modal weights of all participating modes distribute unequally and, often, there are few modes (e.g., around 1–3 modes) dominating the vibration response (or with higher values of weight). Thereby, we may say that the weight of one participating mode is supposed to be

[1]Corresponding author.

Contributed by the Ocean, Offshore, and Arctic Engineering Division of ASME for publication in the Journal of Offshore Mechanics and Arctic Engineering. Manuscript received October 12, 2011; final manuscript received September 16, 2015; published online October 29, 2015. Editor: Solomon Yim.

originally related to the potential energy of this mode, which can be determined by hydrodynamic force, system damping, and the location where the excitation originally happens. In this study, the multimode VIV of slender riser in different flow fields is examined by finite element method (FEM) simulation. New approaches to determine the modal excitation length are proposed for different flow fields.

In Sec. 2, a numerical simulation model based on FEM is developed, in which the vortex-induced lift coefficient C_L is expressed by a function of the instantaneous motion of structure. This model can avoid costly computation of iteration calculation and is more suitable to time-domain calculation by FEM code. In Sec. 3, the multimode VIV of slender riser, respectively, in stepped and shear flows is examined and compared with experimental results. In the case of stepped flow, effect of reduced velocity on modal weight is explored. Further, a semi-empirical formula describing the relationship between the normalized modal weight and reduced velocity is given. In the case of shear flow, the distribution of the participating modes is discussed. In order to deal with the overlap of excitation region of participating modes, the modal energy, characterizing the competition power of the mode against other participating modes, is used to determine the length and position of modal excitation region. At last, conclusions are given in Sec. 4.

2 Hydrodynamic Model and Finite Element Simulation

2.1 Hydrodynamic Model. The governing equation of a slender riser, of which the structure is generally simplified as a tensioned Euler beam, undergoing VIV can be written as

$$m\frac{\partial^2 y(z,t)}{\partial t^2}+\gamma\frac{\partial y(z,t)}{\partial t}+\mathrm{EI}\frac{\partial^4 y(z,t)}{\partial z^4}-T\frac{\partial^2 y(z,t)}{\partial z^2}=f(z,t) \quad (1)$$

where $y(z,t)$ is the displacement of structure, m and γ are the structural mass and damping per unit length, EI and T are the bending stiffness and axial tension, and $f(z,t)$ is the hydrodynamic force per unit length consisting of the vortex-induced lift force $f_v(z,t)$ and fluid drag force $f_f(z,t)$. It is difficult to directly derive the exact formula for hydrodynamic force and get the solution of VIV because of the complicated nonlinear interaction between fluid and structure and the turbulence character of fluid. Here, it is assumed that the structural motion in lock-in is sinusoidal, i.e., $y=A\sin(\omega t)$, and the vortex-induced lift force, $f_v(z,t)$, is written as

$$f_v(z,t)=(1/2)C_L\rho V^2 D\sin(\omega_v t+\varphi) \quad (2a)$$

The fluid drag force $f_f(z,t)$ can be expressed by virtue of the Morison equation, i.e.,

$$f_f(z,t)=(1/2)C_D\rho D(V-\dot{y})|V-\dot{y}|+(1/4)\pi C_A\rho D^2(\dot{V}-\ddot{y})+(1/4)\pi D^2\rho\dot{V} \quad (2b)$$

where ρ and V are the density and velocity of the fluid, respectively, and ω and ω_v are the frequencies of structure and vortex shedding, respectively. As lock-in occurs, $\omega=\omega_v$ and $\phi=90$ deg. C_L is the vortex-induced lift coefficient and C_D and C_A are the drag and added mass coefficients, respectively, of which the values can be determined by VIV experiment.

The fluid wake field of a riser undergoing VIV is too complicated to directly get a theoretical solution because of the uncertainties like the turbulence, separation, and boundary layer. So, mostly, the lift coefficient C_L in Eq. (2a) is supposed a constant that is independent on structure motion. Recent experimental researches have found that C_L actually is related to the structure motion due to the interaction between fluid and structure dynamics during VIV lock-in [1,6,12]. Further, C_L was presented in terms of nondimensional amplitude A/D, as shown in Fig. 1 [12] where the coordinate values of the key points, such as C_{Lmax}, C_{LA0}, $\bar{A}_0$, and $\bar{A}_{Lmax}$, can be determined based on the experimental data. This approach applies better in frequent domain simulation rather than time-domain simulation. However, for FEM simulation, the numerical simulation is implemented in time-domain but not in frequency domain. Because the response amplitude, A/D, is not yet known before an FEM calculation, a complex iteration process is needed, which is computationally expensive for FEM calculations. Moreover, the calculation process involving such complex iterations in dynamic response simulation is too complicated to be carried out by running our finite element code.

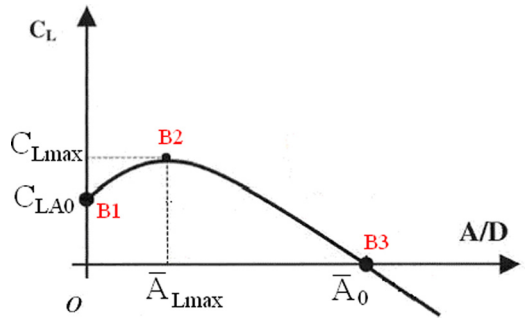

Fig. 1 Lift curve

Here, an alternative lift coefficient expressed by the instantaneous motion of structure, the velocity $\dot{y}$, instead of the final response amplitude A/D, is proposed as follows:

$$C_L(\dot{y})=C_{L0}+a\dot{y}+b\dot{y}^2+c\dot{y}^3 \quad (3)$$

where C_{L0} indicates the lift coefficient when the amplitude is $A/D=0$. The coefficients, a, b, and c, can be derived according to the idea of energy equality to the previous lift curve, as shown in Fig. 1. In other words, the total input energy by the lift force in Eq. (3) is supposed to equal to the energy by the previous lift force in Fig. 1 during one vibration period of VIV. Then, the values of a, b, c, and C_{L0} can be solved out by fitting the new curve with the original curve at key points, e.g., points B1, B2, and B3 in Fig. 1. Or, a group of equations describing the relationship between the previous lift force and the new one are as follows:

$$C_{L0}=C_{LA0} \quad (4a)$$

$$C_{L0}\left[1+\omega a\bar{A}_{Lmax}+\frac{8\omega^2}{3\pi}b\left(\bar{A}_{Lmax}\right)^2+\frac{3\omega^3}{4}c\left(\bar{A}_{Lmax}\right)^3\right]=C_{Lmax} \quad (4b)$$

$$\omega a+\frac{16\omega^2}{3\pi}b\bar{A}_{Lmax}+\frac{9\omega^3}{4}c\left(\bar{A}_{Lmax}\right)^2=0 \quad (4c)$$

$$C_L''\left[1+\omega a\bar{A}_0+\frac{8\omega^2}{3\pi}b(\bar{A}_0)^2+\frac{3\omega^3}{4}c(\bar{A}_0)^3\right]=0 \quad (4d)$$

where $\bar{A}_0$ and $\bar{A}_{Lmax}$ are the amplitudes as $C_L=0$ and $C_L=C_{Lmax}$, respectively, as shown in Fig. 1.

2.2 Finite Element Simulations. The governing equation of a riser in FEM simulation can be written as follows [18,19]:

$$\mathbf{M}\ddot{\mathbf{Y}}+\mathbf{C}\dot{\mathbf{Y}}+\mathbf{K}\mathbf{Y}=\mathbf{F}$$

where $\mathbf{M}$, $\mathbf{C}$, and $\mathbf{K}$ are the structural mass, damping, and stiffness matrix, respectively, and $\mathbf{Y}$ and $\mathbf{F}$ are the displacement and load vector of node. The dynamic response of the riser undergoing VIV can be obtained by combining the presented hydrodynamic force and FEM. The vortex-induced lift force $f_v(z,t)$ and the drag

force $f_f(z,t)$ exerted by the ambient fluid are loaded, respectively, at the nodes in the excitation region and the nodes in damping region along the riser length. Element mass is equally divided at two nodes of each beam element.

Since we already have the nonlinear load and central mass in terms of element nodes, direct numerical integration is used to solve the dynamic governing equation. The fundamental structural response (displacement) is solved at discrete times with a fixed integration times step Δt ($\Delta t \leq (1/50)T_{\min}$, where $T_{\min}$ is the minimum natural period of all participating modes. By using a central finite-difference representation for the velocity and the acceleration at discrete times

$$\dot{\mathbf{Y}}_n = \frac{1}{2\Delta t}(\mathbf{Y}_{n+1} - \mathbf{Y}_{n-1}), \quad \ddot{\mathbf{Y}}_n = \frac{1}{\Delta t^2}(\mathbf{Y}_{n+1} - 2\mathbf{Y}_n + \mathbf{Y}_{n-1})$$

the equation of motion can be solved by central finite-difference method so as to effectively run the computation process with acceptable numerical accuracy.

The initial condition is that the initial displacement and velocity are both zero. For the pinned ends of riser, the boundary conditions at the two ends of the riser are

$$x(0,t) = 0 \qquad x(L,t) = 0$$

and

$$\partial^2 x(0,t)/\partial z^2 = 0 \qquad \partial^2 x(L,t)/\partial z^2 = 0$$

To verify the proposed FEM approach, the numerical VIV in uniform flow is compared with the VIV experiments, i.e., a rigid cylinder (tested by Khalak and Williamson [20]) moving in a manner of single-mode vibration and a flexible cylinder (by Trim et al. [15]) moving in manners of single-mode and multimode vibration, respectively. In our numerical simulations, the hydrodynamic coefficients are $C_A = 1.0$ and $C_d = 1.2$, and the corresponding original lift coefficients are $C_L = 0.5 + 1.82A - 1.29A^2 - 0.707A^3$ and $C_L = 0.22 + 1.62A - 2.31A^2 + 0.754A^3$, respectively, for the cases of rigid and flexible cylinders.

For the rigid cylinder, the experiment [20] indicated that there are three branches of response amplitude, i.e., the initial, upper, and lower branches, through lock-in region. Here, the most dangerous case, i.e., the upper branch where the corresponding reduced velocity V_r is 5.33, is considered. The time history of displacement is presented in Fig. 2, where the experimental amplitude, as a comparison, is also plotted as a solid line (only the value of amplitude was presented in Ref. [20]). Figure 2 shows that the calculated amplitude, $A/D = 0.78$, is somewhat lower than the experimental data, $A/D = 0.81$. In addition, the time history curve, displaying an apparent harmonic sinusoid, implies that the VIV response is characterized by a single-mode vibration.

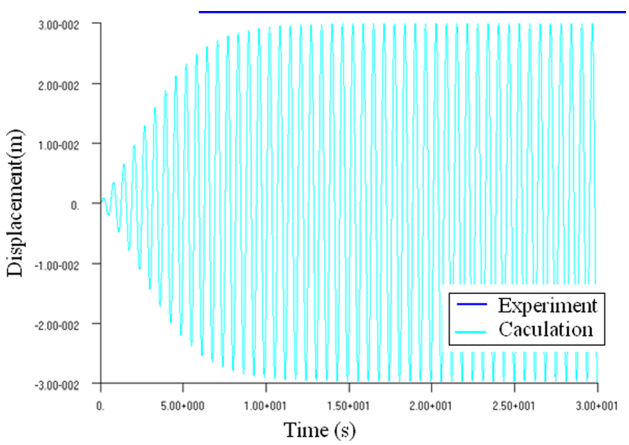

Fig. 2 The displacement response of a rigid cylinder vibrating in a manner of single-mode in uniform flow, the upper line indicates the amplitude of the experimental displacement

For the flexible cable, two cases of dynamic responses, i.e., a single-mode vibration involving only the third mode and a multimode vibration involving the third and fourth modes, are carried out. The numerical results, plotted as the curve of the root-mean-square (RMS) displacement along riser length and the temporal–spatial evolution of displacement, are shown in Figs. 3 and 4, respectively. In the case of single-mode vibration (Fig. 3), only the RMS displacement (Fig. 3(*a*)) near the crests is approximately close to the experimental curve, whereas the displacement, especially near the troughs, diverges distinctly from the experimental curve. Additionally, the calculation curve has apparent nodes of which the displacement nearly equals to zero that means the single-mode vibration is dominated by a standing wave. However, there is no apparent node in the experimental curve. In the case of multimode vibration (Fig. 4), the RMS displacement (Fig. 4(*a*)) agrees better, compared with the single-mode vibration in Fig. 3(*a*), with the experimental curve along the overall length.

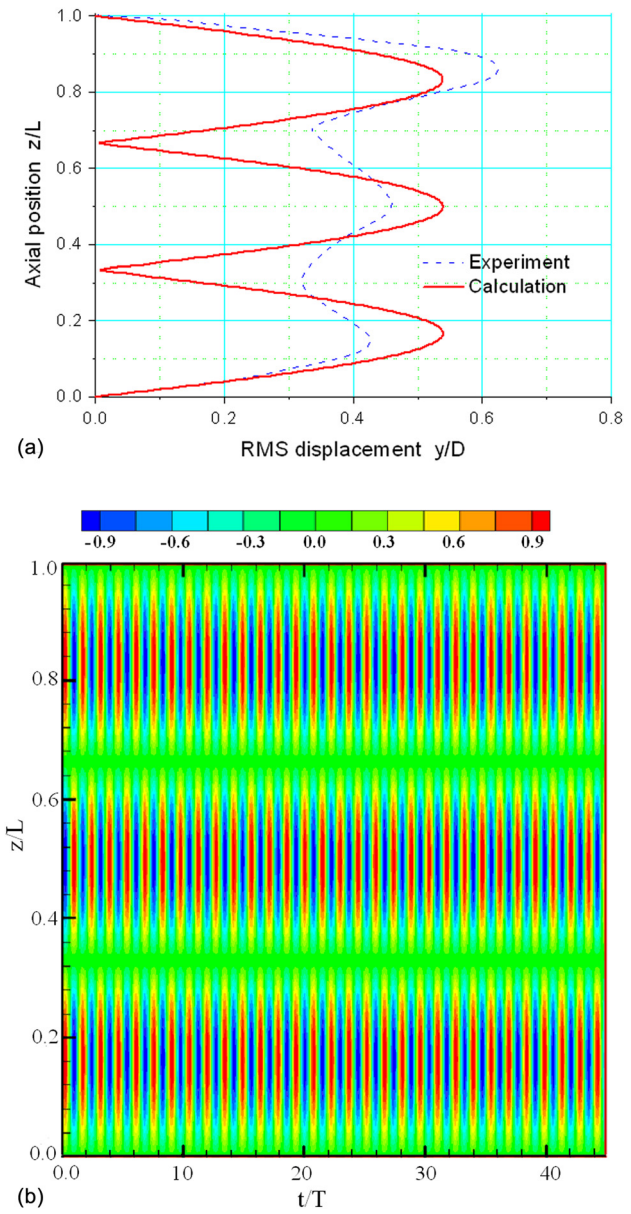

Fig. 3 Comparisons between the presented numerical results and the experimental results of a flexible cylinder vibrating in a manner of single-mode, involving mode 3, in uniform flow: (*a*) the curve of RMS displacement along riser length and (*b*) the temporal–spatial evolution of displacement

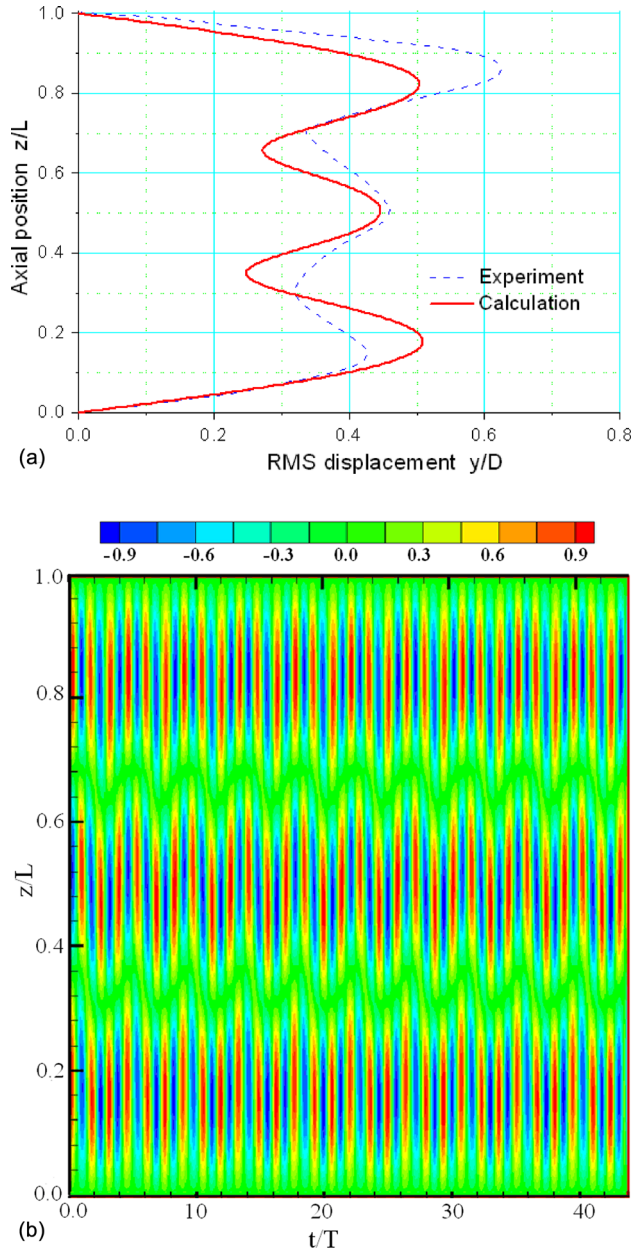

Fig. 4 Comparisons between the presented numerical results and the experimental results of a flexible cylinder vibrating in a manner of single-mode, involving modes 3 and 4, in uniform flow: (*a*) the curve of RMS displacement along riser length and (*b*) the temporal–spatial evolution of displacement

And, a traveling effect is observed in that no evident node appears.

3 Multimode VIV Response and Discussion

One of the challenging problems, which multimode VIV needs to face specifically, is how to determine the modal excitation length for each participating mode. In this section, the multimode vibrations of risers experiencing two kinds of fluid fields, i.e., a stepped flow and a linear shear flow, will be examined. In the case of stepped flow, effect of reduced velocity on modal weight is explored and in the case of shear flow, the distribution of modal weight for the participating modes is discussed.

3.1 VIV in Stepped Flow. First, we consider a simpler case where the flow velocity distributes uniformly along the riser

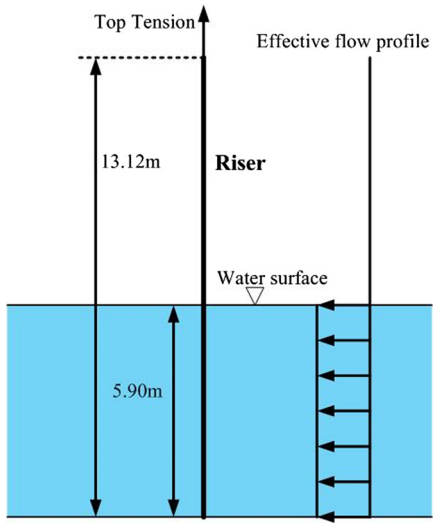

Fig. 5 The experiment of a flexible riser in the stepped flow by Chaplin et al. [16]

length. The previous results [1,2,9,10] of single-mode vibration in uniform indicate that in lock-in region, the response amplitude varies with the increase of flow velocity. Generally speaking, the response amplitude first rises up to reach a peak value and then drops gradually to a small value till the flow velocity is beyond out of lock-in region. Thus, we may say that for a participating mode the flow velocity directly influences its modal response amplitude. Or, in other words, the modal weight mostly depends on the reduced velocity of this mode.

Here, a riser experiencing a stepped flow, shown in Fig. 5, is taken as the object, where the flow velocity uniformly distributes along the portion of length immersed in the fluid. Systematic tests at a series of flow velocity were implemented by Chaplin et al. [16]. And fortunately, the modal weights of participating modes were recorded.

In order to have a deeper insight into the modal excitation distribution, the evolution of modal weight of all the participating modes was observed with respect to the reduced velocity in overall lock-in region. We found, in Figs. 6, 7, and 9 of Ref. [16], that the participating modes vary, in a way of both the value of modal weight and the order number of participating mode, when the reduced velocity increases during the lock-in region. It is also noted that appearance of new excitation mode is usually accompanied with disappearance of previously existing vibrating mode. Or, the newly participating mode that possesses gradually increasing power of competition against others may overcome the one with weaker power till the old one disappears in dynamic response. Three groups of modal weights are listed in Table 1. It shows that there are five modes, i.e., modes 4–8, participating in the dynamic response, and the values of modal weight range from 0.03 to 0.55. The dominating mode (with the largest value of modal weight) is no longer the mode with the highest order number as described in previous methods [4,14].

Further, we normalized these modal weights (divided by the maximum values in each group), then plotted the normalized modal weight against the modal reduced velocity $V_{rn} = V/Df_n$ in Fig. 6. It is noted that among the participating modes, the mode, of which the reduced velocity approximately corresponds to 6–7, mostly tends to dominate the response, or to possess a powerful priority competing against other modes. Another interesting phenomenon is that the vibration enters into lock-in region quickly, or the curve is abrupt as V_r increasing from 4 to 7, whereas the vibration goes out of lock-in region slowly, or the curve becomes flatter as V_r further increases from 7 to 12. To describe the relationship between the normalized modal weight W_n and the modal

Table 1 Experimental measurements of modal weight in the cases of top tension of $T = 1073$ N and $T = 939$ N, respectively

Mode number	Modal weight top tension $T = 939$ N carriage speed $V = 0.85$ m/s	Modal weight top tension $T = 1073$ N carriage speed $V = 0.90$ m/s	Modal weight top tension $T = 958$ N carriage speed $V = 1.00$ m/s
4	0.03	0.08	0.10
5	0.15	0.12	0.15
6	0.25	0.50	0.22
7	0.42	0.28	0.32
8	0.05	0.05	0.55

T = top tension.

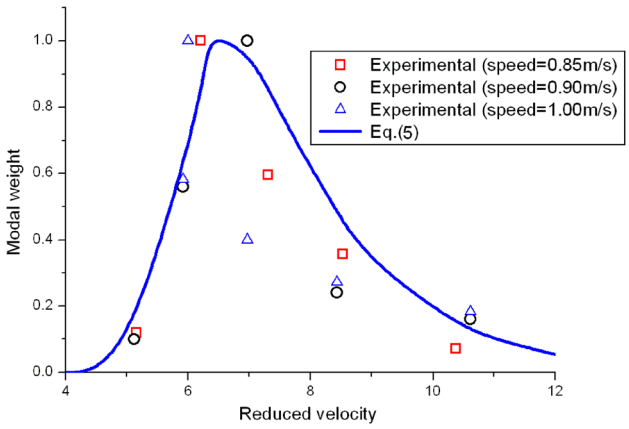

Fig. 6 Effect of reduced velocity on the modal weight

reduced velocity V_{rn}, a curve-fit function (see Fig. 6) is proposed as follows:

$$W_n = \frac{1}{1.2} e^{(-e^{(-z_1)} - z_2 + 1)} \tag{5}$$

where $z_1 = (V_{rn} - 6.0)/0.7$ and $z_2 = (V_{rn} - 6.0)/1.6$. We note that for the case of $V = 1.00$ m/s carriage speed (triangular symbols in Fig. 6), there exist noticeable divergences between the fitting curve and experiment data at reduced velocities $V_{rn} = 6.9$ and 8.2. The reason causing such divergence maybe lie in those unsteady states occurring in the experimental response (reported in Ref. [16]). While, for the other two carriage speeds of $V = 0.90$ m/s and $V = 0.85$ m/s, the experimental response were all measured at steady-state.

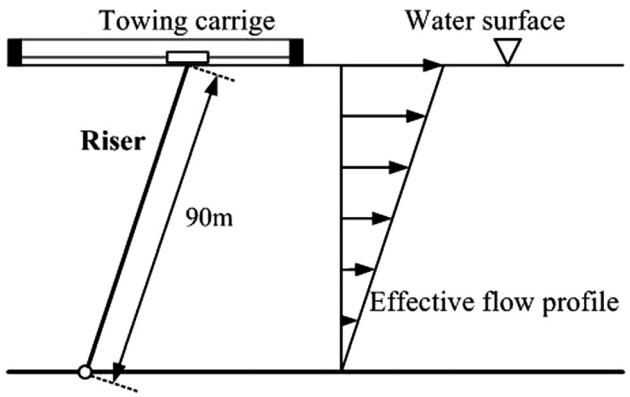

Fig. 8 Experiment of flexible riser experiencing shear flow [13]

The displacement curves at different time steps are plotted and compared with the experiment in Fig. 7. Both numerical and experimental results indicate that the vibration is characterized by a traveling wave, in which the node moves along the rise length rather than staying at a fixed position. Additionally, mode 7 dominates the response and the largest amplitude, nearly up to 1.0, agrees with the experiment.

3.2 VIV in Shear Flow. In practice, some fluid fields, such as ocean current and the flow induced by internal-wave, are usually regarded as shear flow in which the multimode VIV is more complex and will be examined in this section. First, the method to recognize participating mode and determine its excitation region is studied. Then, the VIV response is calculated and compared with the large-scale test by Trim et al. [15] (shown in Fig. 8). Further, the modal weight distribution of the participating modes is discussed.

3.2.1 Determination of the Length of Modal Excitation Region. Initially, since flow velocity $V(z)$ varies linearly along the riser length, the excitation region of participating modes can be naturally determined by the reduced velocity at location z. It is assumed that when the reduced velocity at z for mode n is within the lock-in bandwidth, $V_r = 4.0$–12.0, the location z will belong to the excitation region of this mode. Subsequently, overlaps between adjacent excitation regions will appear if several modes simultaneously participate in the vibration.

To eliminate the overlap, two methods are currently used. One method [4,14] (the high-mode priority) assumes that the regions of lower mode are covered by the regions of higher modes.

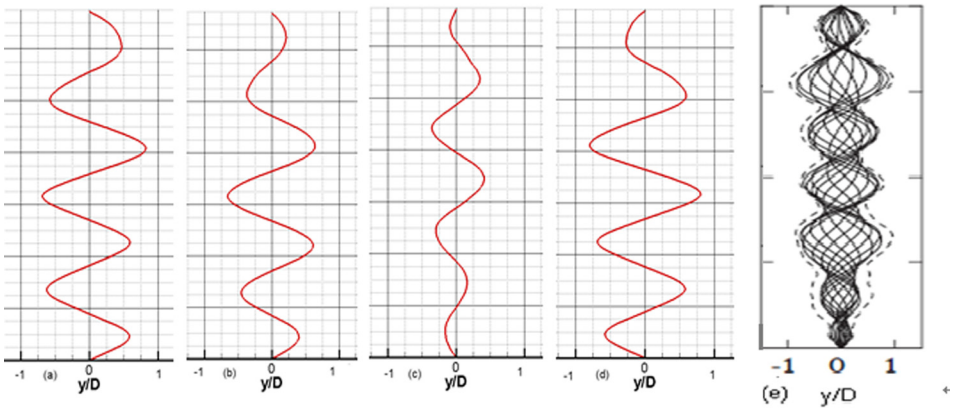

Fig. 7 VIV amplitude of flexible riser experiencing stepped flow by numerical simulation (the left four plots at different time steps) and experiment (the last one by Chaplin et al. [16])

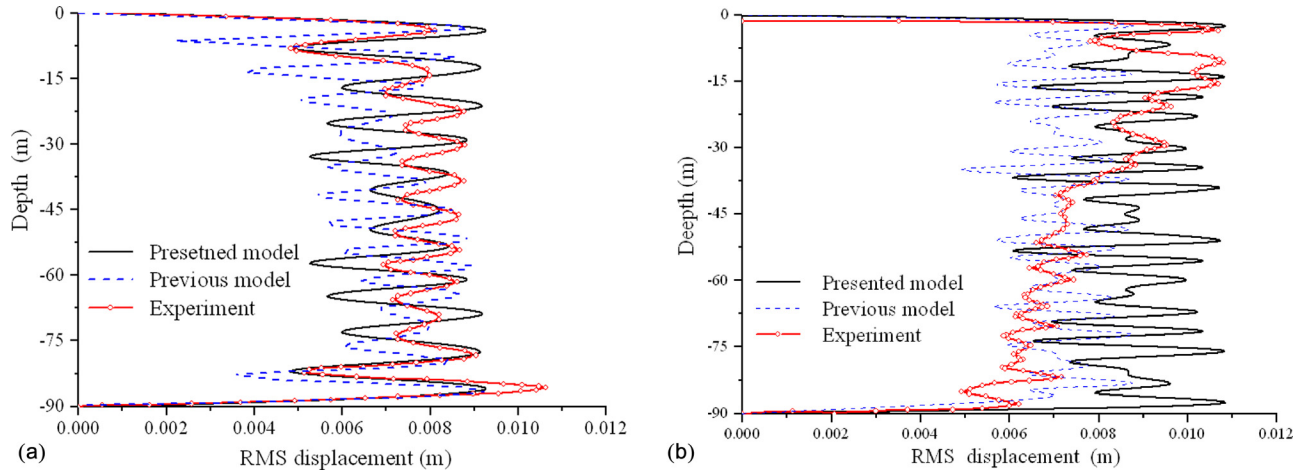

Fig. 9 RMS displacement of flexible riser in shear flow: (*a*) 0.54 m/s towing speed and (*b*) 1.14 m/s towing speed

Another method [12] (the equally shrinking) assumes that the excitation region length of each mode involved in the overlap equally shrinks until the overlap is eliminated. Here, we suggest that the excitation region length of participating modes shrinks, proportionally to its modal energy, till the overlap disappears. In other words, the modal excitation length L_n is assumed to be proportional to it modal energy in a form of

$$L_n/L_m = P_n/P_m \tag{6}$$

The modal energy is written as follows [2,12]:

$$P_n = (F_n)^2/(2R_n) \tag{7}$$

where F_n and R_n are the modal force and damping.

The modal force F_n can be written as

$$F_n = \int_{L_n} (1/2)C_L\rho V(z)^2 D\varphi_n^2(z)dz \tag{8}$$

where $\varphi_n(z)$ is the mode shape of n th mode. Ideally, F_n should depend on structure motion, because the fluid dynamics couples essentially with the structure dynamics as VIV occurs. However, before the numerical simulation the structure motion is not yet known. Thus, at this stage, the lift coefficient C_L is assumed to be a constant value, 0.8, for a flexible riser [12].

The modal damping R_n involving both hydrodynamic damping and structural damping is written as

$$R_n = \int_{L-L_n} r_h(z)\varphi_n^2(z)\omega_n dz + \int_L r_s(z)\varphi_n^2(z)\omega_n dz \tag{9}$$

where L is the total length of riser and $r_h(z)$ and $r_s(z)$ are the hydrodynamic and structural damping per unit length. The second term in the right side of Eq. (9), the structural damping, can be simplified as $2\xi_{Sn}M_n\omega_n$, where M_n is the modal mass and $\omega_n = 2\pi f_n$. The first term in the right side of Eq. (9), the hydrodynamic damping, can be expressed by the semi-empirical formula. Experiments by Vandiver indicated that hydrodynamic damping behaves differently in different ranges of reduced velocity. At lower reduced velocity ($3.5 < V_r < 6.5$), the hydrodynamic damping $r_h(z)$ is

$$r_h(z) = r_{sw} + (1/2)C_{rl}\rho DV(z) \tag{10}$$

where the static damping $r_{sw} = \omega_n\pi\rho D^2(\sqrt{2/\mathrm{Re}_\omega} + C_{sw})$, $\mathrm{Re}_\omega = \omega_n D^2/\upsilon$, υ is the viscous of fluid, and C_{sw} and C_{rl} are the constant coefficients and have values of 0.125 and 0.06, respectively. At higher reduced velocity ($6.5 \le V_r < 12$), $r_h(z)$ is

$$r_h(z) = 0.2\rho V^2/\omega_n \tag{11}$$

3.2.2 The VIV Response. The VIV responses at ten towing speeds were simulated. Here, the selected results, at two towing speeds of 0.54 m/s and 1.14 m/s, are presented.

Considering first the displacement response, the RMS displacement along the riser length calculated by the presented method is shown in Fig. 9. As a comparison, the displacement calculated by the previous model, in which the length of modal excitation region is determined by the rule of high-mode priority, is also plotted in Fig. 9. In the case of 0.54 m/s speed (Fig. 9(*a*)), the span-averaged RMS displacements are, respectively, 0.0073 m (of the presented model) and 0.0067 m (of the previous model) compared to 0.0075 m of the experiment, while the peak-averaged values are, respectively, 0.0090 m (of the presented model) and 0.0083 m (of the previous model) compared to 0.0088 m of the experiment. Therefore, we may say that the displacement responses of presented model are more consistent with the experimental curve than the previous model.

In the case of 1.14 m/s towing speed (Fig. 9(*b*)), the span-averaged RMS displacements are, respectively, 0.0084 m (of the presented model) and 0.0069 m (of the previous model) compared to 0.0078 m of the experiment, while the peak-averaged values are, respectively, 0.0097 m (of the presented model) and 0.0082 m (of the previous model) compared to 0.0081 m of the experiment. More specifically, the calculated displacement agrees better with the experimental displacement in the excitation region, i.e., the length location is from $z/L = 0.0$ to 0.40, whereas the displacement becomes larger as it approaches the bottom end of the riser. Such a difference is supposed to be caused by the dominating wave. Since the calculated vibration is characterized mainly by a standing wave, the displacement does not attenuate along the overall riser length, while the experimental displacement attenuates as approaching the bottom end of riser due to an effect of traveling wave.

To our understanding, the wave character, such as standing wave or traveling wave, of a response mainly depends on structural properties (like aspect ratio, damping ratio, and mode order number) and fluid factors (like reduced velocity and excitation region). Generally, traveling wave is more likely to happen to a riser with larger values of aspect ratio, damping ratio, and modal order. In the case of multimode VIV, additional reasons like participating modes should be considered. One of the possible reasons of the difference between our and experimental results might be that not all the participating modes, in terms of their modal

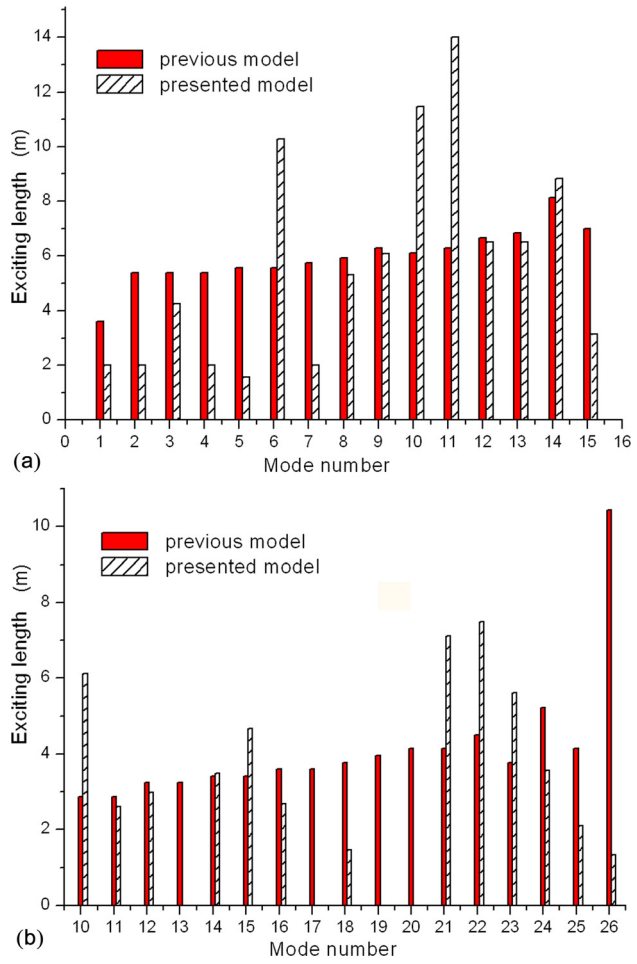

Fig. 10 Length of lock-in region for participating modes: (*a*) 0.54 m/s towing speed and (*b*) 1.14 m/s towing speed

weights and excitation locations, of our simulations exactly agree with the experimental ones.

Considering then the dominating mode, generally speaking, the dominating mode determined by the presented model is consistent with the experimental result. For example, Fig. 9(*a*) (0.54 m/s towing speed) indicates that the dominating modes of both the presented model and experiment are mode 11, however, the dominating mode determined by the previous model is mode 14.

Now, considering the modal excitation region, the modal excitation lengths of all participating modes are presented in Fig. 10 and also compared with the previous model. It is seen that the modal excitation length no longer averagely distributes as it does in the previous model. Taking the case of 0.54 m/s towing speed as an example (Fig. 10(*a*)), there are approximately three groups of participating modes, i.e., mode 6, modes 10 and 11, and mode 14. However, by the previous model, all the participating modes have almost equal excitation length, except the highest mode which has a pronounced large length due to its highest mode number (Fig. 10(*b*)). Subsequently, since all participating modes have approximately same level of excitation power, it is difficult to exclude the mode of which the vibration is, in practical response, too weak to be considered. Therefore, there may be more participating modes included in the previous model than the presented model. This phenomena can be seen in Fig. 10(*b*), where 17 modes, modes 10–26, are include in the previous model, whereas modes 13, 17, 19, and 20 does not participate in the vibration in the presented model.

At last, we would like to discuss a bit on VIV prediction and its improvement. On the one hand, we tried to improve our VIV approach by means of considering the coupling between fluid and structural dynamics and modal competition and developed a coupled hydrodynamic model along with a modified method of lock-in region based on modal energy. On the other hand, it is worthwhile to point out that the experimental data used for the lift coefficients are important for the accuracy of dynamic response. For multimode VIV, among the VIV experiments, the results based on the situations, such as a cylinder freely vibrating or flexible cable (with large aspect ratio) rather than forced vibration or rigid body, are strongly recommended, e.g., the experiments of Refs. [6–8,12,13,16,17].

4 Conclusions

A time-domain analysis approach for VIV of deepwater risers, using finite element simulation combined with a hydrodynamic model coupling with structure motion, is developed. VIV responses of slender risers, respectively, in stepped and shear flows are explored. Compared with the previous model, better agreement of displacement response with experiment is observed. Based on our numerical results, we draw the following conclusions:

(1) For multimode VIV in stepped flow, modal excitation region is mostly influenced by reduced velocity. A semi-empirical formula describing the relationship between the normalized modal weight W_n and the reduced velocity $V_{rn} = V/Df_n$ is given in Eq. (5).
(2) For multimode VIV in shear flow, modal excitation region can be determined by modal energy, and the participating modes approximately distribute after a manner of scattering groups.

Because this approach is based on an empirical lift curve, it still does not fully capture the physics behind VIV especially some strongly nonlinear phenomena, such as the jump of displacement in different branches and the hysteresis in lock-in region. Further works on more reasonable hydrodynamic model and appropriate coupling between the fluid and structure should be considered.

Acknowledgment

This work was supported by the Intellectual Innovation Project of the Chinese Academy of Sciences (Grant No. KJCX2-YW-L07) and the National Natural Sciences Foundation (Grant Nos. 11232012 and 11372320).

References

[1] Sarpkaya, T., 2004, "A Critical Review of the Intrinsic Nature of Vortex-Induced Vibration," J. Fluids Struct. Mech., **19**(4), pp. 389–447.
[2] Vandiver, J. K., 1993, "Dimensionless Parameters Important to the Prediction of Vortex-Induced Vibration of Long, Flexible Cylinders in Ocean Currents," J. Fluids Struct., **7**(5), pp. 423–455.
[3] Moe, G., and Arntsen, O., 2001, "VIV Analysis of Risers by Complex Modes," 11th International Offshore and Polar Engineering Conference, Vol. 3, pp. 426–430.
[4] Lyons, G. J., and Patel, M. H., 1986, "A Prediction Technique for Vortex Induced Transverse Response of Marine Risers and Tethers," J. Sound Vib., **111**(3), pp. 467–487.
[5] Facchinetti, M. L., de Langre, E., and Biolley, F., 2004, "Vortex-Induced Traveling Waves Along a Cable," Eur. J. Mech. B/Fluids, **23**(1), pp. 199–208.
[6] Huarte, F. J. H., Bearman, P. W., and Chaplin, J. R., 2006, "On the Force Distribution Along the Axis of a Flexible Circular Cylinder Undergoing Multi-Mode Vortex-Induced Vibrations," J. Fluids Struct., **22**(6–7), pp. 897–903.
[7] Huse, E., Kleiven, G., and Nielsen, F. G., 1998, "Large Scale Model Testing of Deep Sea Risers," Offshore Technology Conference, Houston, TX, May 4–7, Paper No. OTC 8701.
[8] Huse, E., Kleiven, G., and Nielsen, F. G., 1999, "VIV-Induced Axial Vibration on Deep Sea Risers," Offshore Technology Conference, Houston, TX, May 3–6, Paper No. OTC 10932.
[9] Grant, R., Litton, R., Finn, L., Maher, J., and Lambrakos, K., 2000, "Highly Compliant Rigid Risers: Field Test Benchmarking a Time Domain VIV Algorithm," Offshore Technology Conference, Houston, TX, May 1–4, Paper No. OTC 11995.
[10] Dong, S., and Karniadakis, G. E., 2005, "DNS of Flow Past a Stationary and Oscillating Cylinder at Re = 10,000," J. Fluids Struct., **20**(4), pp. 519–531.

[11] Yamamoto, C. T., Meneghini, J. R., and Saltara, F., 2004, "Numerical Simulations of Vortex-Induced Vibration on Flexible Cylinders," J. Fluids Struct., **19**(4), pp. 467–489.
[12] Vandiver, J. K., 2002, "A Universal Reduced Damping Parameter for Prediction of Vortex-Induced Vibration," ASME Paper No. OMAE2002-28292.
[13] Lie, H., and Kaasen, H. K., 2006, "Model Analysis of Measurements From a Large-Scale VIV Model Test of a Riser in Linearly Sheared Flow," J. Fluid Struct., **22**(4), pp. 557–575.
[14] Chen, W. M., Zhang, L. W., and Li, M., 2009, "Prediction of Vortex-Induced Vibration of Flexible Riser Using an Improved Wake-Oscillator Model," ASME Paper No. OMAE2009-79336.
[15] Trim, A. D., Braaten, H., and Lie, H., 2005, "Experimental Investigation of Vortex-Induced Vibration of Long Marine Risers," J. Fluids Struct., **21**(3), pp. 335–361.
[16] Chaplin, J. R., Bearman, P. W., Huarte, F. J. H., and Pattenden, R. J., 2005, "Laboratory Measurements of Vortex-Induced Vibrations of a Vertical Tension Riser in a Stepped Current," J. Fluids Struct., **21**(1), pp. 3–24.
[17] Larsen, C. M., Vikestad, K., Yttervik, R., and Passano, E., 2001, "Empirical Model for Analysis of Vortex Induced Vibrations-Theoretical Background and Case Studies," ASME Paper No. OMAE2001/OFT-1203.
[18] Park, H. I., and Jung, D. H., 2002, "A Finite Element Method for Dynamic Analysis of Long Slender Marine Structures Under Combined Parametric and Forcing Excitations," Ocean Eng., **29**(11), pp. 1313–1325.
[19] Chen, W. M., Li, M., and Zheng, Z. Q., 2012, "Dynamic Characteristics and VIV of Deepwater Riser With Axially Varying Structural Properties," Ocean Eng., **42**, pp. 7–12.
[20] Khalak, A., and Williamson, C. H. K., 1999, "Motions, Forces and Mode Transitions in Vortex-Induced Vibrations at Low Mass-Damping," J. Fluids Struct., **13**(7–8), pp. 813–851.